Supporting Information

Triazine-Cored Donor-Acceptor Covalent Organic Framework Promotes Highly Efficient Photoscatalytic Synthesis of H_2O_2

Lihua Li[a*†], Xin Yao[a†], Weizhi Ou[a], Jing Chai[a], Ru Ma[a], Chenglong Ran[a], Anzhi Ma[a], Xiaojun Shi[a], Pifeng Wei[b], Hong Dong[c], Hongpeng Zhou[d*], Wenbing Yang[e], Hai-Chao Hu[e], Jian-Feng Wu[e], Hui Peng[a], Guofu Ma[a*]

[a] Key Laboratory of Eco-functional Polymer Materials of the Ministry of Education, Key Laboratory of Polymer Materials of Gansu Province, College of Chemistry and Chemical Engineering, Northwest Normal University, Lanzhou 730070, China.

[b] School of Chemistry & Chemical Engineering, Linyi University, Linyi, 276000, China.

[c] Heilongjiang Provincial Key Laboratory of CO_2 Resource Utilization and Energy Catalytic Materials, School of Material Science and Chemical Engineering, Harbin University of Science and Technology, Harbin 150040, PR China.

[d] Key Laboratory of Low-Dimensional Quantum Structures and Quantum Control of Ministry of Education, Institute of Interdisciplinary Studies, Key Laboratory for Multifunctional Ionic Electronic Materials and Devices of Hunan Normal University, Changsha 410081, China.

[e] State Key Laboratory of Low Carbon Catalysis and Carbon Dioxide Utilization, Lanzhou Institute of Chemical Physics, Chinese Academy of Sciences, Lanzhou

730000, Gansu, China.

† These authors contributed to the work equally.

*corresponding email addresses: lilihua202109@163.com; hpzhou@hunnu.edu.cn; magf@nwnu.edu.cn

Experimental Section

1. Materials and Instrumentation

Materials 1,3,5-Tris(4-formylphenyl)benzene (TPB-CHO), 4,4',4''-(1,3,5-Triazine-2,4,6-triyl)trianiline ($TPT-NH_2$) and 1,3,5-Tris(4-aminophenyl)benzene ($TPB-NH_2$) were purchased from Jilin Chinese Academy of Sciences Yanshen Technology Co., Ltd. (China). 5,5-dimethylpyrroline *N*-oxide (DMPO), *β*-carotene, *p*-benzoquinone, nitrotetrazolium blue chloride (NBT) and 1,3-diphenylisobenzofuran (DPBF) were bought from Energy Chemical. All the chemicals involved in this work were utilized without further purification.

Instruments The powder X-ray diffraction (PXRD) characterization was collected on D8 ADVANCE with Cu Kα radiation (λ = 1.5405 Å) with a 2θ range from 1.8° to 30° at room temperature. Fourier transform infrared (FT-IR) Spectra were recorded on the Bruker ALPHA FT-IR Spectrometer, ranging from 500 to 4000 cm^{-1}. Solid-state ^{13}C cross-polarization magic angle spinning (CP/MAS) NMR spectra were collected by an Agilent-NMR-vnmrs600. Thermogravimetric analysis (TGA) was carried out on Perkin-Elmer TGA-7 in N_2 atmosphere at 10 °C min^{-1} from 30 °C to 800°C. Scanning electron microscopy (SEM) images were recorded on a Carl Zeiss-Ultra Plus. Transmission electron microscopy (TEM) analysis was conducted on the Hitachi HT7700 electron microscope. The Brunauer-Emmett-Teller (BET) surface areas were tested on an ASAP 2020/TriStar 3000 (Micromeritics) at 77 K. Ultraviolet-visible (UV-Vis) spectra were performed on a Shimadzu UV-2700 spectrophotometer. Luminescent decay curves were measured on the FLS1000 fluorescence spectrophotometer (Edinburgh Instruments). Electron paramagnetic resonance (EPR) measurements were recorded on the Bruker EMXplus-6/1 instrument. The *in-situ* diffuse reflectance infrared Fourier transform (DRIFT) spectra were collected by Bruker Tensor 27 spectrometer. X-ray photoelectron spectroscopy (XPS) spectra were obtained from PHI Versaprobe.

Synthesis of COFs

1.1 Synthesis of TPB-TPT-COF

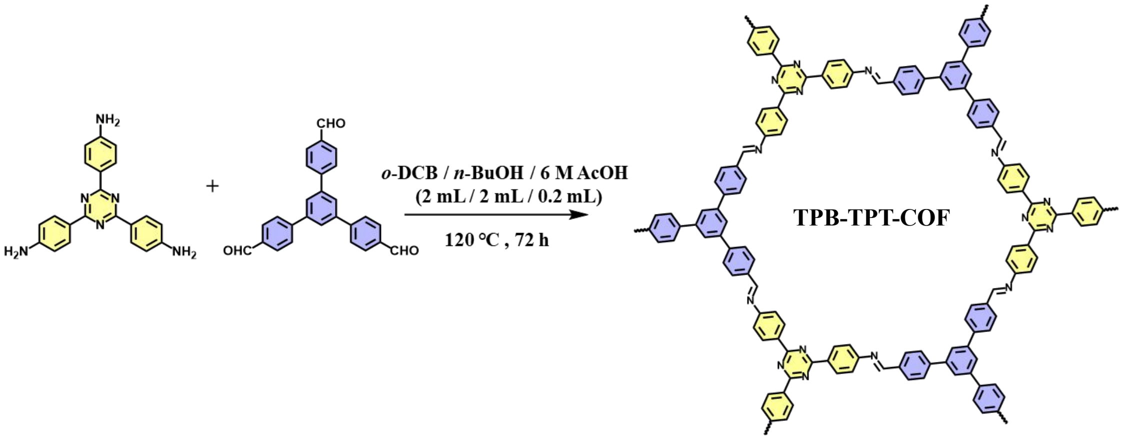

TPB-CHO (0.15 mmol, 58.6 mg), TPT-NH_2 (0.15 mmol, 53.2 mg), *o*-DCB (2 mL), and *n*-BuOH (2 mL) were put into a 10 mL ampoule tube and sonicated. Then, 0.2 mL of AcOH (6 M) was added to the above system, and the ampoule tube was sealed after three freeze-pump-thaw cycles. After being heated at 120 °C for 3 days, the mixture was filtered and washed 6 times with tetrahydrofuran (THF) and acetone. The yellow precipitate was then subjected to Soxhlet extraction with THF for 24 h and dried under vacuum. The powder was obtained with a yield of 85%.[1]

1.2 Synthesis of TPB-COF

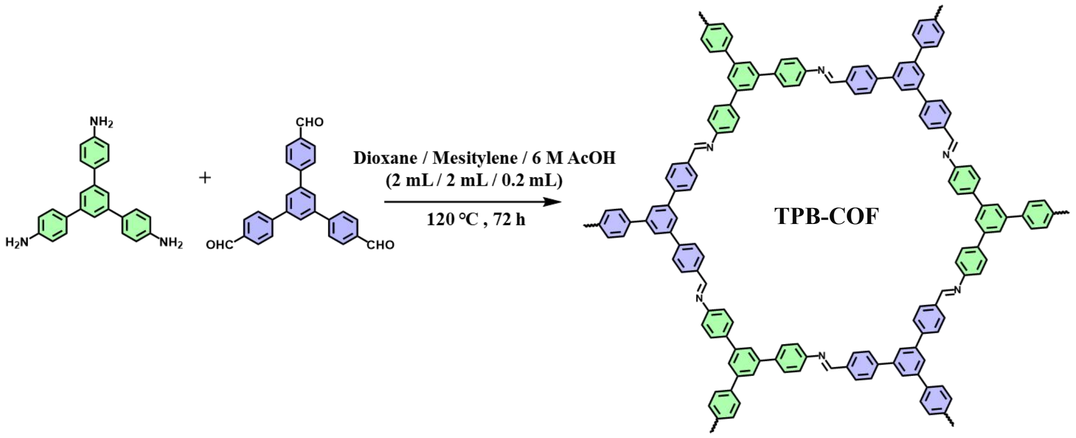

TPB-CHO (0.1 mmol, 39.0 mg), TPB-NH_2 (0.1 mmol, 35.1 mg), Dioxane (2 mL), and Mesitylene (2 mL) were put into a 10 mL ampoule tube and sonicated. Then, 0.2 mL of AcOH (6 M) was added into the above system, and the ampoule tube was sealed after three freeze-pump-thaw cycles. After being heated at 120 °C for 3 days, the mixture was filtered and washed 6 times with THF and acetone. The yellow precipitate was then subjected to Soxhlet extraction with THF for 24 h and dried under vacuum. The powder was obtained with a yield of 86%.[2]

2. *In-situ* diffuse reflectance infrared Fourier transform spectroscopy (DRIFTS)

In-situ diffuse reflectance infrared Fourier transform spectroscopy (DRIFTS) measurements were performed using a Nicolet iS50 Fourier-transform spectrometer equipped with a Harrick diffuse reflectance accessory at the Infrared Spectroscopy. After N_2 gas sweeps the sample for 30 min, water vapor and O_2 were purged into the reactor with the sample in the dark, and the container was closed after the ventilation was stopped. The N_2 was purged and sweeps the sample for 30 min, after a 300 W xenon lamp (> 420 nm) was used to illuminate the sample with vapor and N_2 purging.

3. Structure simulations and powder X-ray diffraction (PXRD) analyses:

Table S1: The cell parameters of TPB-TPT-COF and TPB-COF.

Name	*a*	*b*	*c*	*α*	*β*	*γ*
TPB-TPT-COF	27.01	26.18	3.75	90°	90°	120°
TPB-COF	26.27	25.99	3.84	90°	90°	120°

4. Structure modelling. Structural modeling and Pawley refinement were performed using structural refinement software, and crystal structure determination was conducted based on XRD patterns. The corresponding space groups were identified from the Reticular Chemistry Structure Resource. Subsequently, the theoretical models were optimized utilizing the Forcite module. Pawley refinements of the PXRD patterns were carried out within the Reflex module over a 2θ range of 2.5° to 40°, showing good agreement with the simulated patterns of AA stacking models.

5. DFT calculation. First-principles DFT calculations were carried out to investigate the reaction mechanism of oxygen reduction reaction and water oxidation on COFs. All of the calculations were performed using the projector-augmented wave (PAW) method as implemented in the Cambridge Sequential Total Energy Package (CASTEP). The energy cutoff for the plane-wave basis expansion was set to 500 eV. And the generalized gradient approximation (GGA) with the Perdew-Burke-Ernzerhof (PBE) exchange-correlation functional was used. The self-consistent electron density was determined using iterative diagonalization of the Kohn–Sham Hamiltonian, with the occupation of the Kohn–Sham states being smeared according to a Fermi–Dirac distribution with a smearing parameter of $k_{BT} = 0.1$ eV. Gas phase H_2O and H_2 were used as reference states because they are readily treated and the poor description of the ground state of the O_2 and H_2O_2 molecules in DFT calculations. For all of the calculations, the convergence criteria were set as 10^{-5} eV for electronic loops and 0.01 eV $Å^{-1}$ for ionic loops. The Brillouin zone of the bulk structures was sampled using a 1 × 1 × 7 uniform k-point mesh. A vacuum region of about 20 Å is used to eliminate interlayer interaction.[3-5]

6. Photocatalytic H_2O_2 production. 5 mg of catalysts and 20-60 mL of water were put in an unsealed device mainly composed of a quartz tube. The suspension was well dispersed by ultrasonication for 5 min and O_2 was bubbled into the suspension for 30 min in the dark. Prior to the photocatalytic tests, the suspension was stirred for 30 min in dark to reach the absorption desorption equilibrium. The reaction system was irradiated by a Xe lamp with a cut-off filter (CHL-HXF300-T3, $\lambda > 420$ nm). The concentration of H_2O_2 was determined by UV-vis spectrophotometer. For example, aft er irradiation at different times (0.5-3 h), 3 mL of liquid was sampled and filtrated with a 0.22 μm filter to further remove the photocatalysts. The sample was mixed with pre-prepared of 0.4 M KI and 0.1 M potassium hydrogen phthalate ($C_8H_5KO_4$) solution and the concentrations of H_2O_2 was determined by the UV-vis spectrophotometer.

7. H_2O_2 detection method. The amount of H_2O_2 was determined by iodometry according to the previous reported method.[6] Specifically, potassium iodide (KI) solution (1 mL, 0.4 mol L^{-1}) and potassium hydrogen phthalate ($C_8H_5KO_4$) solution (1 mL, 0.1 mol L^{-1}) were added to a diluted solution (3 mL) and kept for 60 min. H_2O_2 was reacted with I^- under acidic conditions to form I_3^- ($H_2O_2 + 3I^- + 2H^+ \rightarrow I_3^- + 2H_2O$), which has a strong absorption at about 350 nm by UV-vis spectroscopy. The total amount of H_2O_2 produced during the reaction can be calculated. The following image shows the standard curve of H_2O_2 (S10).

8. Photoelectrochemical measurements. Mott-Schottky measurements were performed in Na_2SO_4 solution (0.5 M) through the traditional three electrode system in the CHI 760E electrochemical workstation. Photocurrent and EIS were tested in Na_2SO_4 solution (0.5 M, pH 7). The working electrode is FTO glass plate coated with catalyst slurry, the counter electrode was platinum foil, and saturated Ag/AgCl as the reference electrode. Mott-Schottky plots were measured at alternating current (AC) frequencies of 500 Hz, 1000 Hz, and 1500 Hz. Working electrode preparation: 2 mg of catalyst, 1 mL of ethanol, and 10 μL of Nafion were mixed and sonicated for 30 min. 200 μL of slurry was deposited evenly on the FTO glass plate (1×2 cm^2), which was dried at 60 °C for 6 h.

9. Rotating disk electrode (RDE) measurements. A rotating disk electrode (KERUITE Corporation) was served as the substrate for the working electrode. To prepare the catalyst ink, 2 mg of catalysts were dispersed in a mixture of 1 mL of ethanol and 10 μL of Nafion solution (5 wt%) and then subjected to ultrasonic treatment to ensure homogeneity. A volume of 200 μL of the slurry was placed on the disk electrode and dried at room temperature. The linear sweep voltammograms (LSV) was recorded on an electrode rotator (KERUITE Instrument) and the CHI 760E workstation (Chenhua Instruments, China), with a Pt wire and Ag/AgCl electrodes serving as the counter and reference electrodes, respectively. The LSV were obtained in an O_2-saturated 0.1 M phosphate buffer solution (PBS, pH = 7) solution at room temperature with a scan rate of 10 mV s^{-1} and different rotation speeds. The average number of electrons (n) was calculated by the Koutecky-Levich equation:[7]

$$\frac{1}{J}=\frac{1}{J_L}+\frac{1}{J_K}=\frac{1}{B_{\omega_{1/2}}}+\frac{1}{J_K} \qquad \text{(Eq. S1)}$$

$$B=0.62nFC_0D_0^{2/3}v^{-1/6} \qquad \text{(Eq. S2)}$$

where J is the measured current density, J_K and J_L are the kinetic and diffusion-limiting current densities, ω is the angular velocity, n is transferred electron number, F is Faraday constant (96485 C mol^{-1}), C_0 is the bulk concentration of O_2 (1.26×10^{-6} mol cm^{-3}), D_0 is the diffusion coefficient of O_2 in 0.1 M phosphate buffer solution (2.7×10^{-5} cm^2 s^{-1}), and v is kinetic viscosity of the electrolyte (0.01 cm^2 s^{-1}), respectively.

10. Electrons spin resonance (ESR) measurements. 2 mg of COFs (TPB-TPT-COF and TPB-COF, respectively) and 2 mL of methanol (containing DMPO 100 mM) were added into a quartz tube. The signals were collected under darkness and irradiation by a 300 W Xe lamp with a cut-off filter ($\lambda \geq 420$ nm) for 5 min under the O_2 atmosphere.

2 mg of COFs (TPB-TPT-COF and TPB-COF, respectively) and 2 mL of water (containing TEMP 100 mM) were added into a quartz tube. The signals were collected under darkness and irradiation by a 300 W Xe lamp with a cut-off filter ($\lambda \geq 420$ nm) for 5 min under the O_2 atmosphere.

2 mg of COFs (TPB-TPT-COF and TPB-COF, respectively) and 2 mL of water (containing TEMP 100 mM and benzoquinone 0.1 mM) were added into a quartz tube. The signals were collected under darkness and irradiation by a 300 W Xe lamp with a cut-off filter ($\lambda \geq 420$ nm) for 5 min under the O_2 atmosphere.

11. Detect $O_2^{\bullet-}$ by NBT. 1 mg of COFs (TPB-TPT-COF and TPB-COF, respectively) and 8 mL of NBT solution (0.05 mM) were mixed and dispersed in a quartz tube. The quartz tube was illuminated by a 300 W Xe lamp (Perfect Light PLS-SEX 300D) and cooled by circulating water. After irradiation at different times (0 min, 10 min, 20 min, 30 min, 40 min, and 50 min, respectively), the supernatant was collected by centrifugation, and the UV-Vis spectra were collected.

12. Detect $O_2{}^1$ by DPBF. 1 mg of COFs (TPB-TPT-COF and TPB-COF, respectively), 4 mL of water, and 4 mL of DPBF solution (0.05 mM, DMF as solvent) were mixed and dispersed in a quartz tube. The quartz tube was illuminated by a 300 W Xe lamp (Perfect Light PLS-SEX 300D) and cooled by circulating water. After irradiation, the supernatant was collected by centrifugation, and the UV-Vis spectra were collected.

13. Apparent quantum yield measurements. The measurement of apparent quantum efficiency (AQY) was similarly carried out according to literature.[8] The photocatalytic reaction was carried out in pure deionized water (50 ml) with photocatalyst (5 mg) in a foil reflective light-concentrating reactor. After ultrasonication and Air bubbling, the bottle was irradiated by an Xe lamp (light intensity at 420-700 nm). The optical power was determined by a PL-MW 2000 photoradiometer (Beijing Perfect Light Technology Co., Ltd., Beijing, China). For Calculation of the apparent quantum yield (AQY), the incident light was monochromated by band-pass glass filters.

Calculation of the apparent quantum yield (AQY):

$$AQY = \frac{(\text{number of } H_2O_2 \text{ production}) \times 2}{\text{number of incident photons}} \times 100\% \qquad \text{(Eq. S3)}$$

The number of incident photons is:

$$N_{incident} = \frac{Pt}{hv} = \frac{Pt\lambda}{hc} = \frac{ISt\lambda}{hc} \qquad \text{(Eq. S4)}$$

Where, *h* is the Planck constant (6.626 × 10^{-34} J s), *c* is the speed of light (3× 10^8 m s^{-1}), *I* is the intensity of the irradiation light (mW cm^{-2}), *S* is the irradiation area (cm^2), *t* is the photoreaction time (s), and *λ* is the wavelength of the monochromatic light (nm).

14. Determination of SCC efficiency. For solar-to-chemical conversion (SCC), a UV cut filter (λ > 420 nm) was used to avoid decomposition of the formed H_2O_2 by absorbing UV light.

$$SCC\,(\%) = \frac{[\Delta G\ for\ H_2O_2\ generation\ (J\ mol^{-1})][H_2O_2\ formed\ (mol)]}{[total\ input\ power\ (W)][reaction\ times\ (s)]} \times 100\% \qquad \text{(Eq. S5)}$$

where ΔG = 117 kJ mol^{-1}. For example, when using TPB-TPT-COF as the catalyst, the irradiated sample areas are 19.625 cm^2 during 60 min of illumination

15. Photocatalytic oxygen production. The reaction was tested in a closed reactor, which was connected with a closed gas system. 10 mg of the catalyst was dispersed in 50 mL of 0.01 M $AgNO_3$ solution. and 100 mg of La_2O_3 was added into the system to adjust the pH value. During the reaction, the catalytic system was purged with Ar until it was in an oxygen-free state. And O_2 was generated under the irradiation of visible light ($\lambda \geqslant 420$ nm). The generated O_2 was detected by on-line gas chromatography.

16. Isotope labelling experiments. Mix 5 mg of the catalyst with 0.5 mL of $H_2{}^{18}O$ (97%) and 2 mL of a 0.01 M $AgNO_3$ aqueous solution, and transfer the mixture to a sealed quartz vial with a capacity of 10 mL. Then, the suspension was obtained by ultrasonication. Pure Ar was bubbled into the suspension for 30 min in the dark. After 10 h irradiation, the gas products in the headspace of the reaction vessel were collected and analyzed by MS.

17. Cycling tests. Take 50 mg of COF material and conduct a 1-hour light irradiation reaction in an environment of oxygen and pure water. After the reaction is completed, separate the photocatalyst by centrifugation, wash it with ethanol, and then place it in a 70 °C vacuum drying oven for drying for 12 hours. Subsequently, take 5 mg from the remaining COF material for the cycling experiment and record the yield data once every 1 hour. Continue the photocatalytic reaction on the remaining COF material, repeat the centrifugation, washing and drying steps, and take 5 mg again for the cycling experiment. Repeat this process to complete a total of 5 cycling experiments.

18. Supplementary Figures and Tables

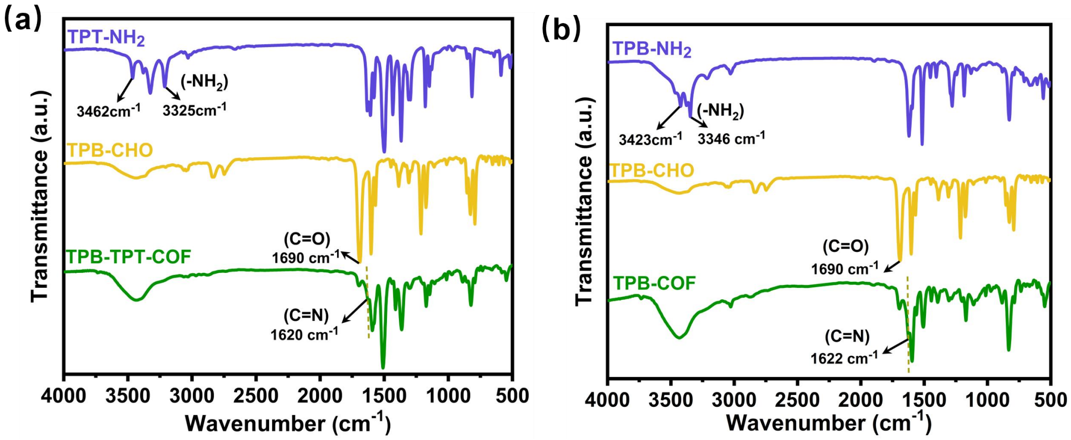

Figure S1. The FT-IR spectra of TPB-TPT-COF and TPB-COF.

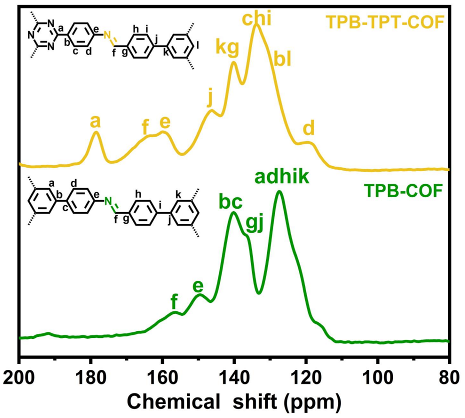

Figure S2. Solid-state ^{13}C-ssNMR spectra of TPB-TPT-COF and TPB-COF.

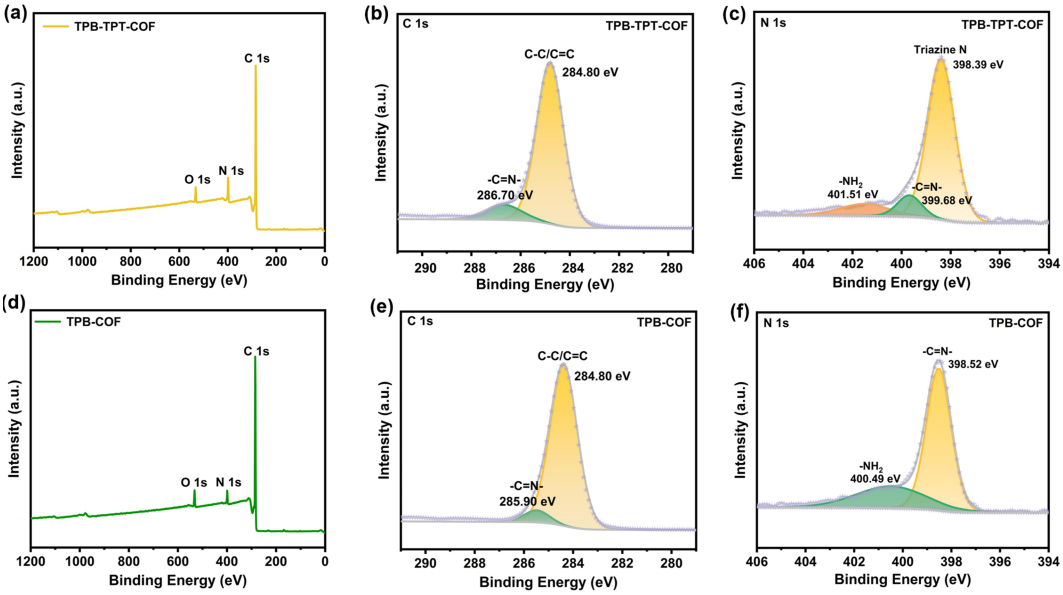

Figure S3. XPS survey spectra (a) and high-resolution XPS spectra of C 1s (b) and N 1s (c) for TPB-TPT-COF and XPS survey spectra (d) and high-resolution XPS spectra of C 1s (e) and N 1s (f) for TPB-COF.

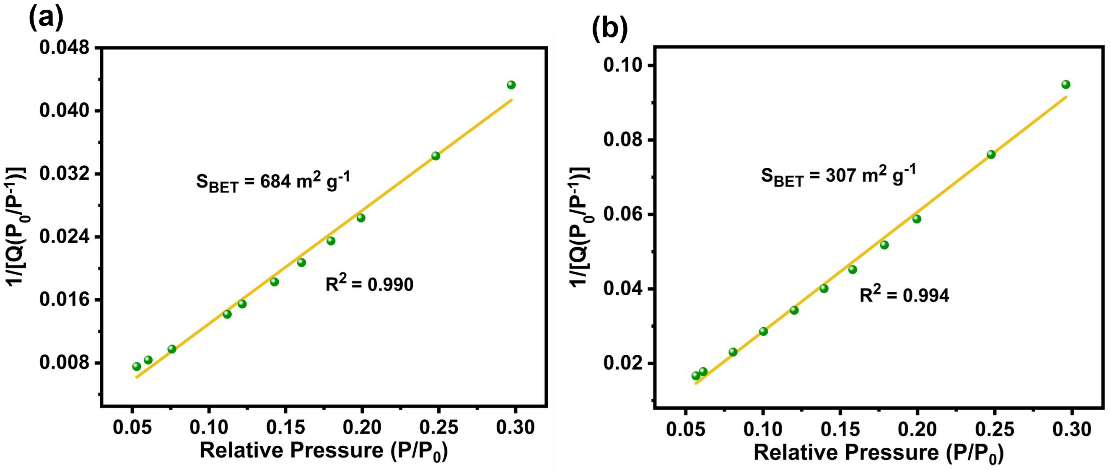

Figure S4. BET surface area maps of TPB-TPT-COF and TPB-COF.

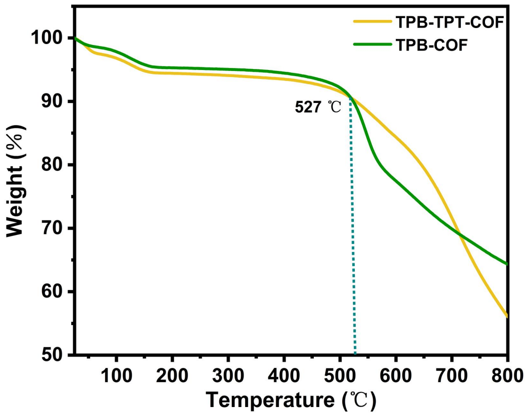

Figure S5. TGA curves of TPB-TPT-COF and TPB-COF.

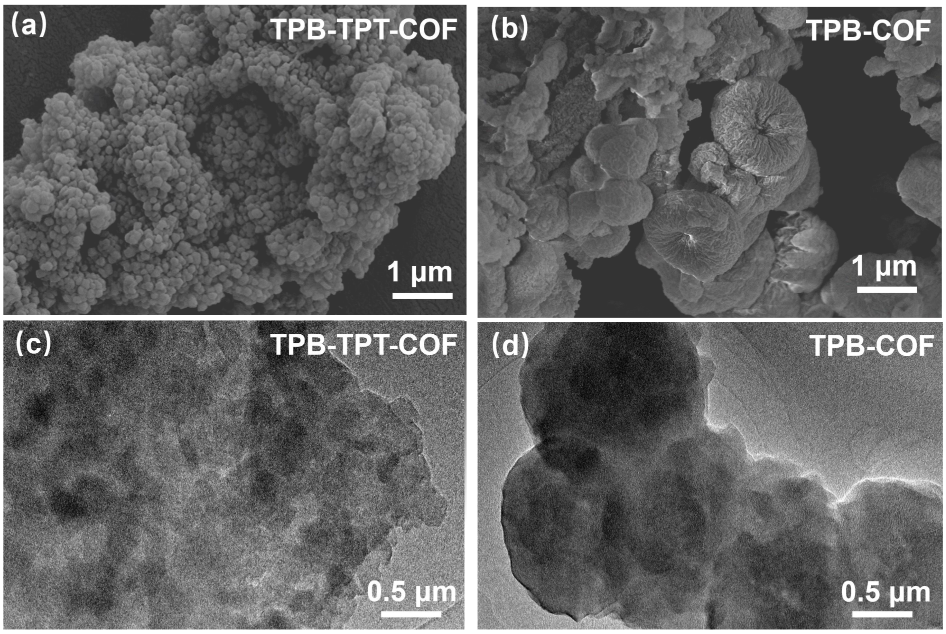

Figure S6. SEM and TEM image of COFs: (a, c) TPB-TPT-COF and (b, d) TPB-COF.

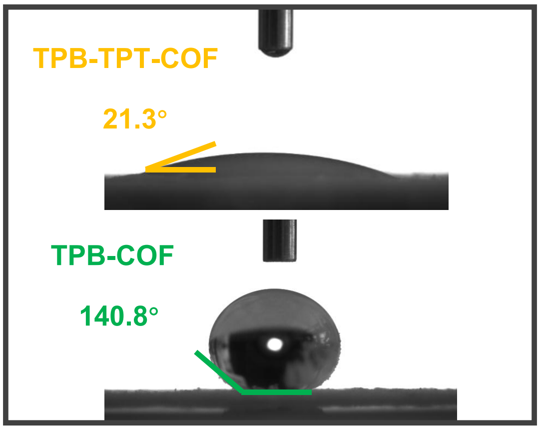

Figure S7. Contact angles of TPB-TPT-COF and TPB-COF.

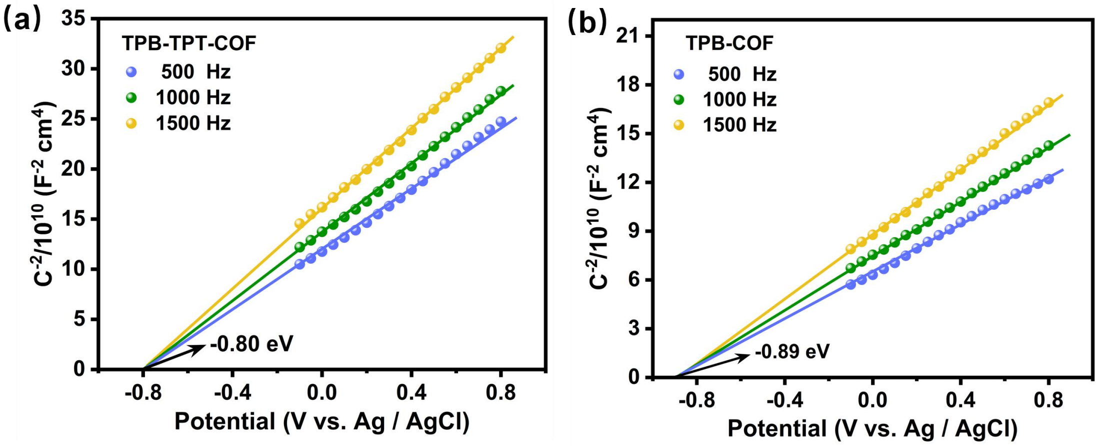

Figure S8. Mott−Schottky plots of (a) TPB-TPT-COF and (b) TPB-COF.

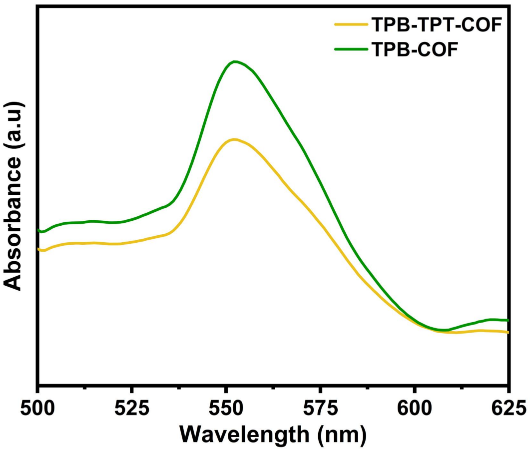

Figure S9. PL spectra of TPB-TPT-COF and TPB-COF.

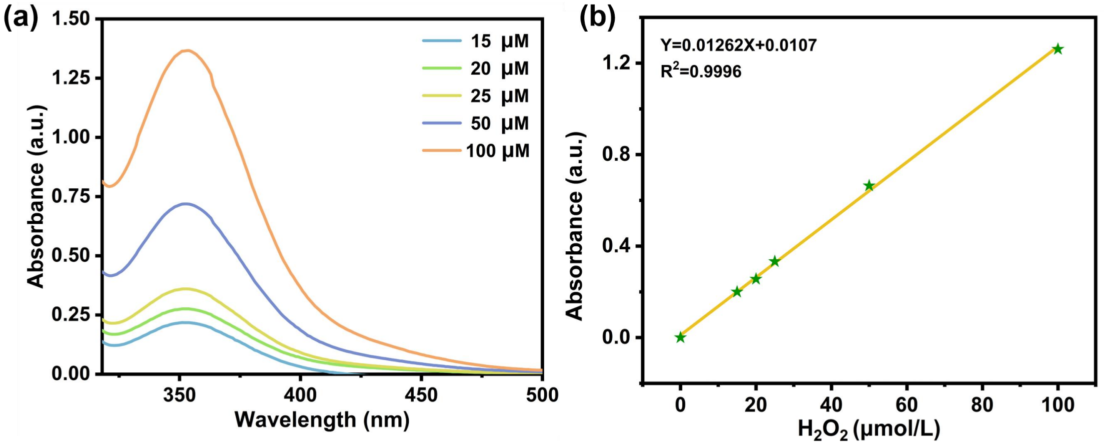

Figure S10. (a) The UV spectra and (b) the standard curve of H_2O_2 concentration-absorbance by the iodometry.

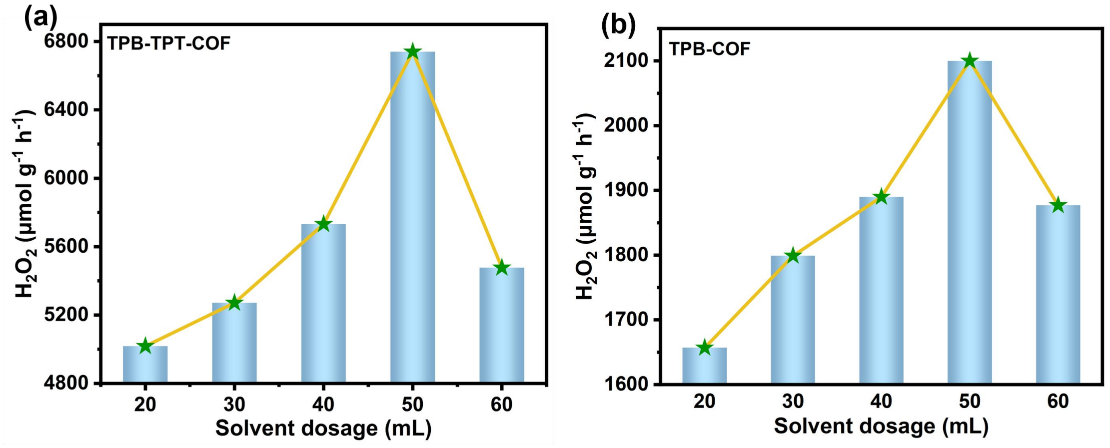

Figure S11. Effects of dosages of (a) TPB-TPT-COF and (b) TPB-COF on H_2O_2 photogeneration performances under air and pure water condition.

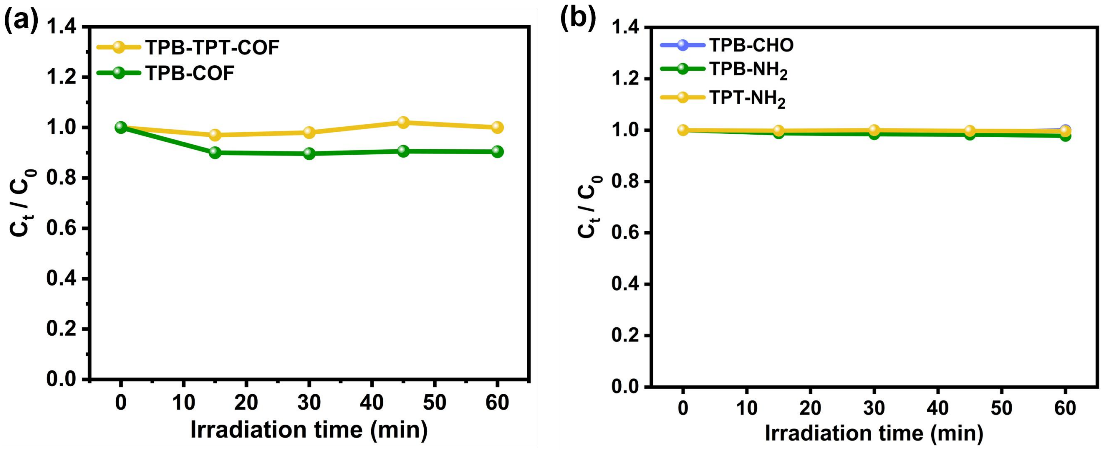

Figure S12. (a) The decomposition of H_2O_2 by COFs; (b) The decomposition of H_2O_2 by monomers of COFs. Reaction condition: 5 mg monomers in 50mL 200 μM H_2O_2, $\lambda > 420$ nm 300 W Xe lamp.

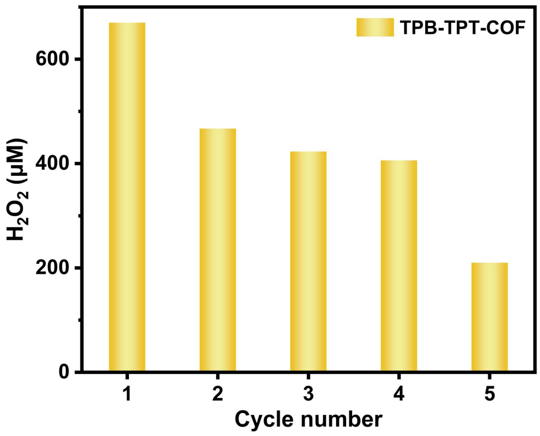

Figure S13. H_2O_2 photoproduction rates for five catalytic cycles of TPB-TPT-COF.

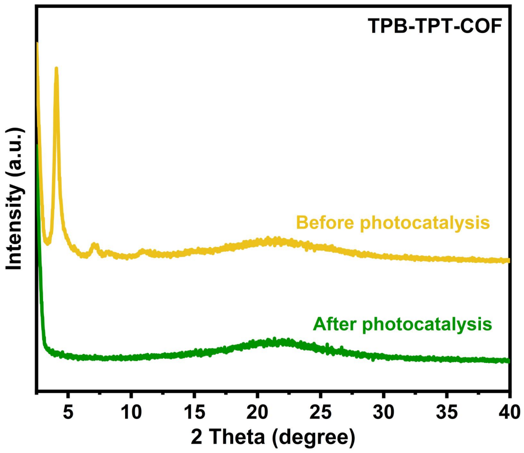

Figure S14. PXRD patterns of TPB-TPT-COF before and after 5 consecutive photocatalytic cycles.

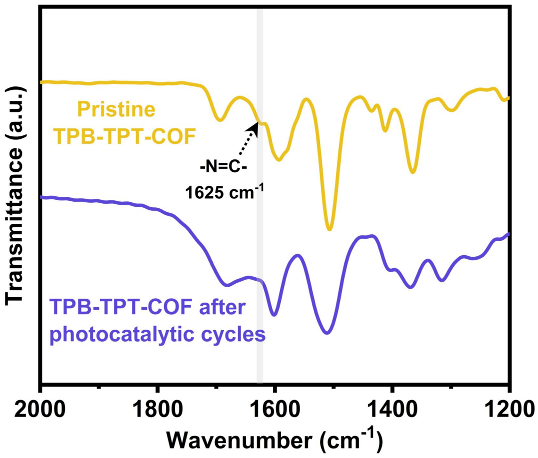

Figure S15. FT-IR patterns of TPB-TPT-COF before and after 5 consecutive photocatalytic cycle.

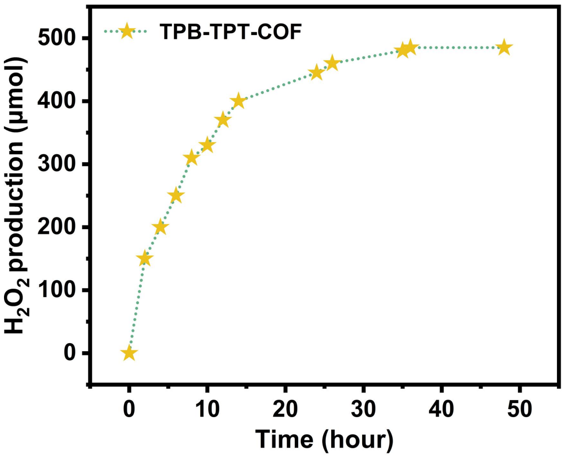

Figure S16. Long-term photocatalytic experiment for TPB-TPT-COF under an O_2-saturated atmosphere (50 mg catalyst in 50 mL water under visible light, λ>420 nm).

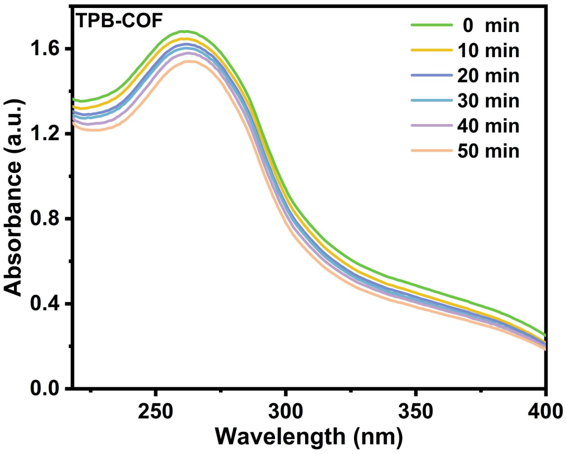

Figure S17. Detecting $\bullet O_2^-$ in the TPB-COF photocatalytic systems by NBT.

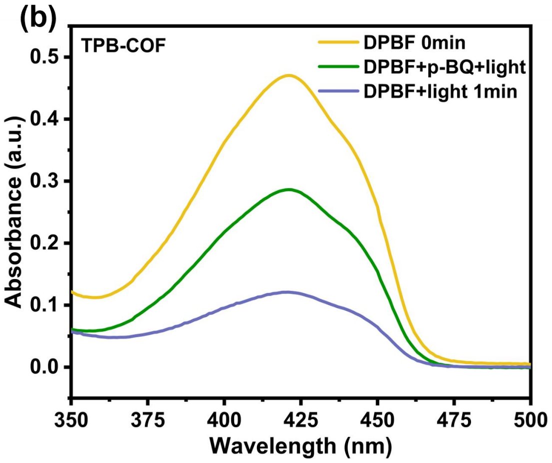

Figure S18. Detecting O_2^1 in the TPB-COF photocatalytic systems by DPBF.

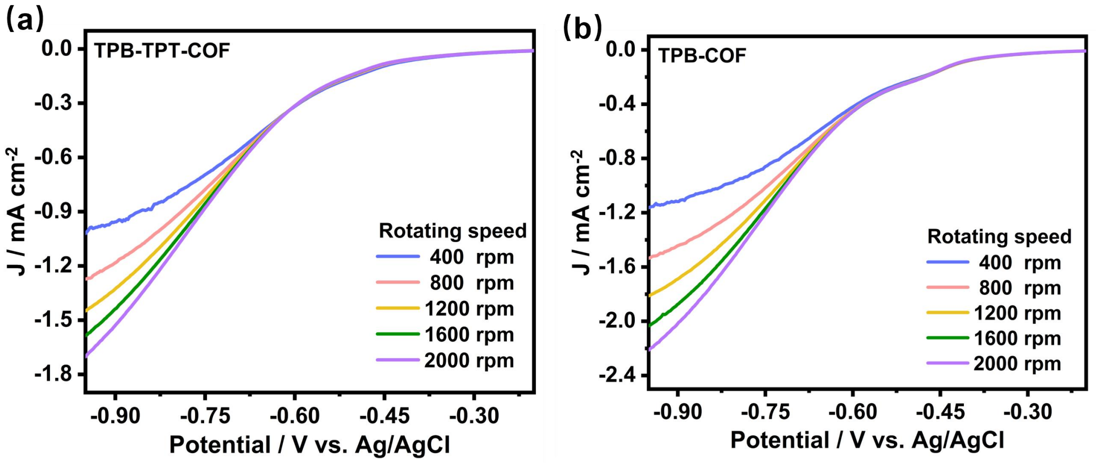

Figure S19. LSV curves using RDE for (a) TPB-TPT-COF and (b) TPB-COF in rotating speeds from 400 rpm to 2000 rpm.

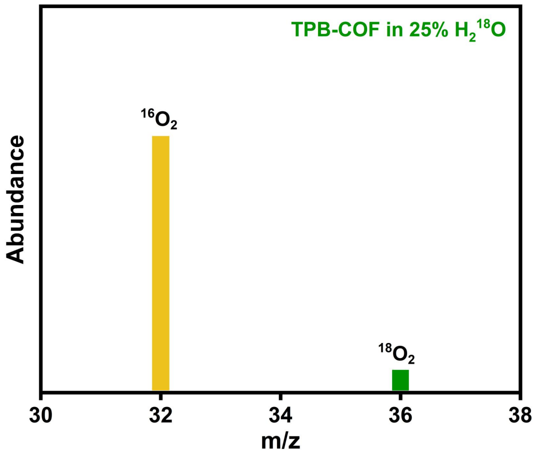

Figure S20. $H_2{}^{18}O$ isotope labelling experiment of TPB-COF.

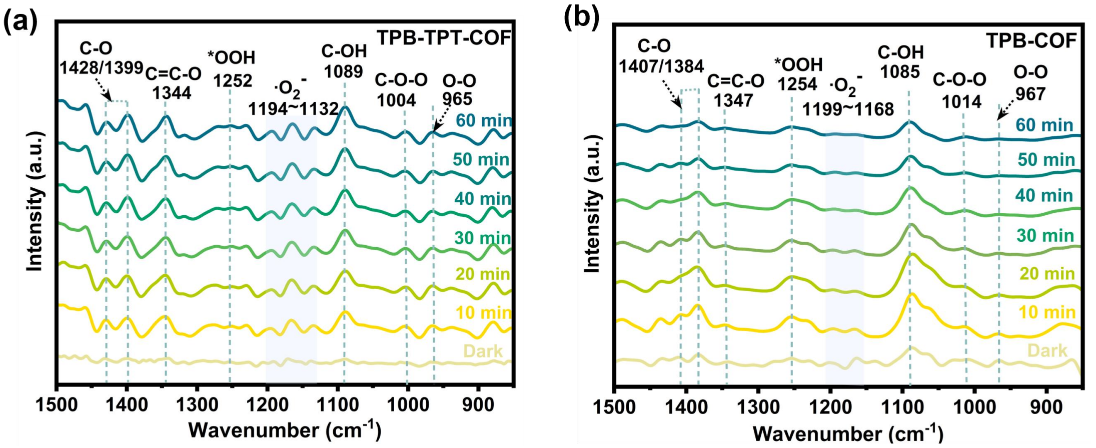

Figure S21. *In-situ* DRIFT spectra of (a)TPB-TPT-COF and (b)TPB-COF recorded during photocatalytic H_2O_2 evolution. *In-situ* DRIFTS of TPB-COF shows similar peak positions to TPB-TPT-COF. However, under the same conditions, the •O_2^-

intermediate peak of TPB-COF was much weaker than that of TPB-TPT-COF (Figure S21). Moreover, the peak values of important intermediates decreased with the increase of time. It is speculated that after the active site on the surface of the catalytic material was adsorbed by the product, the adsorption amount of subsequent reactants decreased, and the functional group signals related to the active site was weakened accordingly, which may also explain the low yield of TPB-COF.[9]

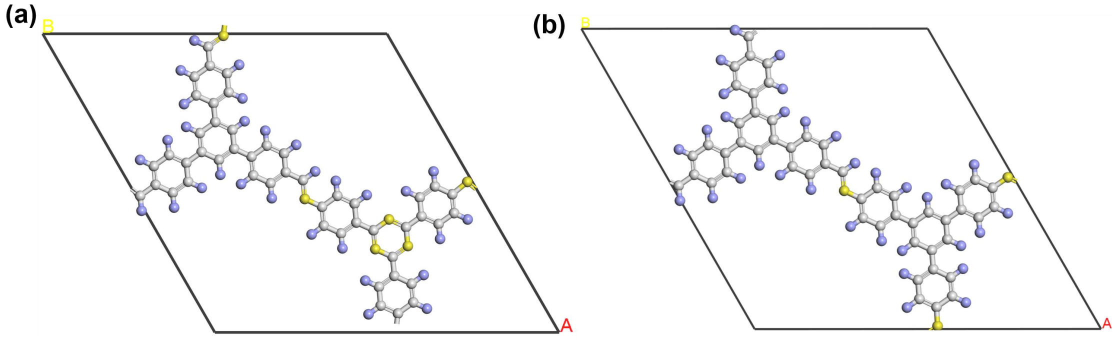

Figure S22. The optimized periodic structures of TPB-TPT-COF and TPB-COF (C, gray; N, yellow; H, blue).

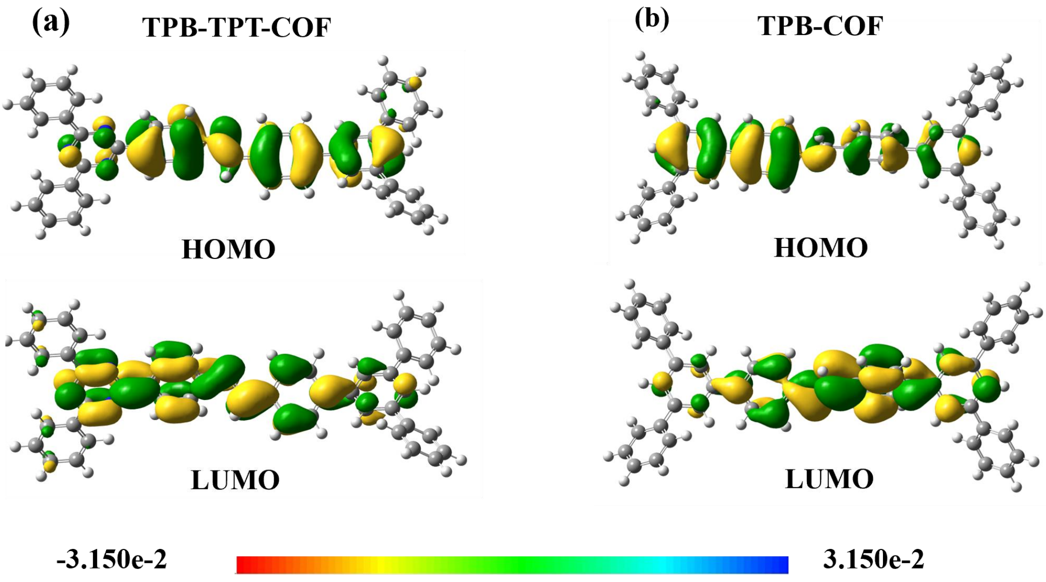

Figure S23. Calculated HOMO and LUMO distribution of periodic unit of (a) TPB-TPT-COF and (b) TPB-COF. Density functional theory (DFT) was used to analyze the catalytic active sites. As can be seen from Figure S22, the highest unoccupied molecular orbital (HOMO) of TPB-TPT-COF is mainly derived from the imine bond and its adjacent benzene ring, and the lowest unoccupied molecular orbital (LUMO) is primarily composed of contributions from the imine bond, as well as its adjacent benzene and triazine rings. According to the distribution characteristics of HOMO-LUMO, the benzene ring near the C=N bond in TPB-TPT-COF can be identified as a potential active site. Similarly, the benzene ring region connected by imine bonds in TPB-COF becomes a potential active site due to the high overlap between HOMO and LUMO and the activity of electron transfer.

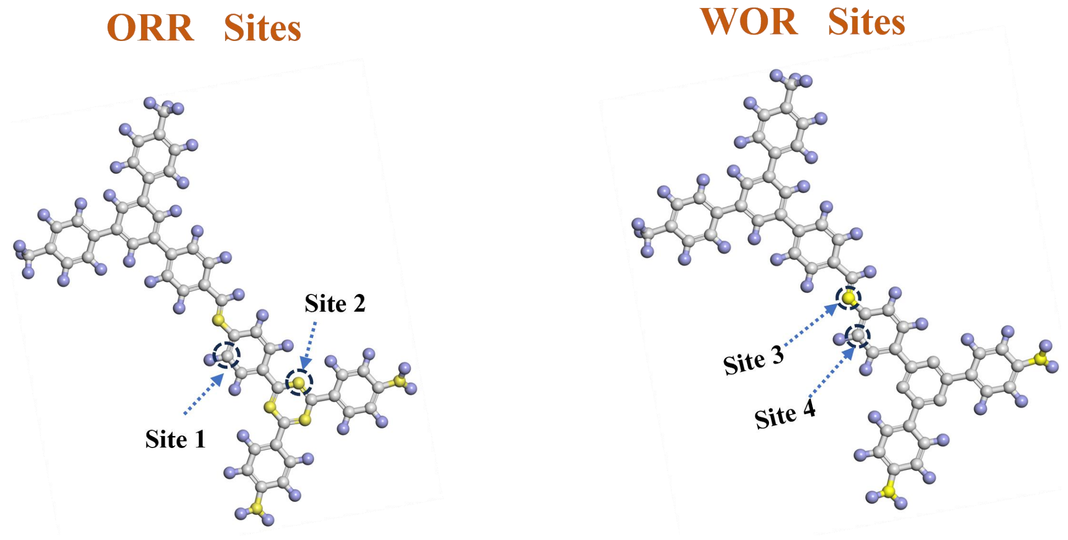

Figure S24. Potential active sites are as follows.

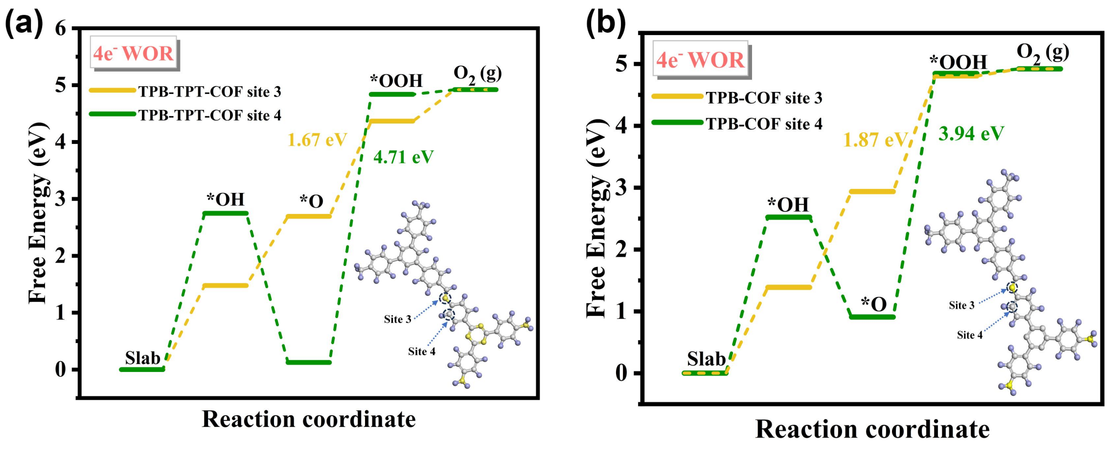

Figure S25. Calculated Gibbs free energy diagram for the water oxidation reaction of two COFs at active sites 3 and 4.

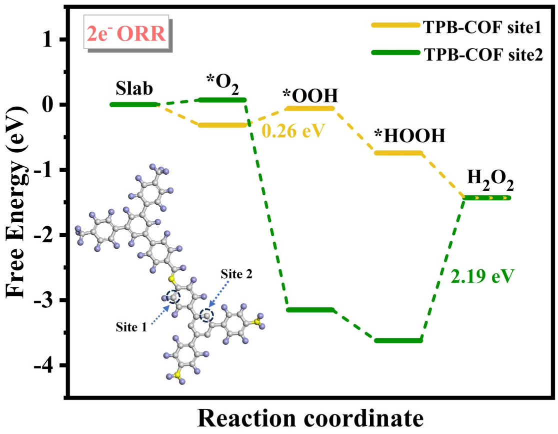

Figure S26. Calculated Gibbs free energy diagram of oxygen reduction reaction on different active sites for TPB-COF.

Table S2: Comparison with other representative materials in H_2O_2 production.

Photocatalyst	COF dosage	Light source	H_2O_2 production (μmol h^{-1} g^{-1})	Reaction solution	AQY (%)	SCC (%)	Ref.
TPB-TPT-COF	5 mg	λ > 420 nm (300 W Xe lamp)	6470	Water (50 mL)	1.05 (400 nm)	0.14 (λ > 420 nm)	This work
TPB -COF	5 mg	λ > 420 nm (300 W Xe lamp)	2030	Water (50 mL)	\	\	This work
NiES-COF-3	10 mg	λ > 400 nm (300 W Xe lamp)	3238	Water : BA (9 : 1)	3.17 (420 nm)	0.07 (AM 1.5G)	10
TP-DPBD$_{30}$-COF	2.5 mg	λ > 420 nm (300 W Xe lamp)	7200	Water (15 mL)	18.0 (420 nm)	0.91 (AM 1.5G)	11
COF-Thz	2 mg	λ > 420 nm (300 W Xe lamp)	3701	Water (40 mL)	2.1 (400 nm)	0.13 (300 mw/cm^{-2})	12
TaptBtt	15 mg	λ > 420 nm (300 W Xe lamp)	1407	Water (50 mL)	4.6 (450 nm)	0.296 (AM 1.5G)	13
TAPT-DHA	5 mg	AM 1.5 (300 W Xe lamp)	1629	Water (25 mL)	7.79 (450 nm)	\	14
BBT-ACN COF-1	5 mg	λ > 420 nm (300 W Xe lamp)	2500	Water (50 mL)	3.19 (420 nm)	\	15
N$_3$-COF	10 mg	λ > 420 nm (300 W Xe lamp)	4881	Water (50 mL)	1.5 (420 nm)	0.413 (AM 1.5G)	16
N$_0$-COF	10 mg	495 nm LED	1570	Water (20 mL)	\	\	17

TMT-TT-COF	10 mg	λ > 420 nm (300 W Xe lamp)	1952	Water (30 mL)	\	\	18
USTB-10-S	2.5 mg	λ > 420 nm (300 W Xe lamp)	5041	Water (25 mL)	4.98 (400 nm)	0.06 (AM 1.5G)	19
COF-N32	25 mg	λ > 420 nm (300 W Xe lamp)	605	Water (50 mL)	6.2 (459 nm)	0.31	20
Pylm-BT_F	10 mg	λ > 420 nm (300 W Xe lamp)	5342	Water : IPA (9 : 1)	2.7 (420 nm)	\	21
EBA-COF	10 mg	~ 420 nm 50 W LED	1830	Water : EtOH (9 : 1)	4.4 (420 nm)	\	22
TTF-BT-COF	5 mg	λ > 420 nm (300 W Xe lamp)	2760	Water (10 mL)	11.19 (420 nm)	0.49	23
CHF-DPDA	40 mg	λ > 420 nm (300 W Xe lamp)	1725	Water (20 mL)	16.0 (420 nm)	0.78 (AM 1.5G)	24
HEP-TAPT-COF	50 mg	λ > 420 nm (300 W Xe lamp)	1750	Water (100 mL)	15.35 (420 nm)	0.65 (AM 1.5G)	25
CN-COF	5 mg	λ > 400 nm (300 W Xe lamp)	2623	Water : EtOH (9 : 1)	9.8 (420 nm)	\	26
TT-T-COF	5 mg	λ > 420 nm (300 W Xe lamp)	10066	Water : BA (9 : 1)	19.25 (420 nm)	\	27
2,5-DhaTph	10 mg	λ > 420 nm (300 W Xe lamp)	2103.1	Water : EtOH (9 : 1)	0.15 (450 nm)	\	28
FS-OHOMe-COF	10 mg	λ > 420 nm (300 W Xe lamp)	2000	Water (20 mL)	9.6 (420 nm)	0.58 (AM 1.5G)	29
CTF-TPCZ	100 mg	λ > 420 nm (300 W Xe lamp)	3764	Water (1 L)	4.38 (400 nm)	0.68 (AM 1.5G)	30

References

1. J. Yang, A. Acharjya, M. Y. Ye, J. Rabeah, S. Li, Z. Kochovski, S. Youk, J. Roeser, J. Grüneberg, C. Penschke, M. Schwarze, T. Wang, Y. Lu, R. van de Krol, M. Oschatz, R. Schomäcker, P. Saalfrank and A. Thomas, *Angew. Chem. Int. Ed.*, 2021, **60**, 19797-19803.
2. G. Jiang, W. Zou, Z. Ou, L. Zhang, W. Zhang, X. Wang, H. Song, Z. Cui, Z. Liang and L. Du, *Angew. Chem. Int. Ed.*, 2022, **61**, e202208086.
3. T. D. Kühne, M. Iannuzzi, M. Del Ben, V. V. Rybkin, P. Seewald, F. Stein, T. Laino, R. Z. Khaliullin, O. Schütt, F. Schiffmann, D. Golze, J. Wilhelm, S. Chulkov, M. H. Bani-Hashemian, V. Weber, U. Borštnik, M. Taillefumier, A. S. Jakobovits, A. Lazzaro, H. Pabst, T. Müller, R. Schade, M. Guidon, S. Andermatt, N. Holmberg, G. K. Schenter, A. Hehn, A. Bussy, F. Belleflamme, G. Tabacchi, A. Glöß, M. Lass, I. Bethune, C. J. Mundy, C. Plessl, M. Watkins, J. VandeVondele, M. Krack and J. Hutter, *J. Chem. Phys.*, 2020, **152**, DOI: 10.1063/5.0007045.
4. S. Grimme, J. Antony, S. Ehrlich and H. Krieg, *J. Chem. Phys.*, 2010, **132**, DOI:10.1063/1061.3382344.
5. T. Lu and F. Chen, *J. Comput. Chem.*, 2011, **33**, 580-592.
6. C. Li, H. Xie, S. Zhou, H. Hu, G. Chen, Z. Wei, J. Jiang, J. Qin, Z. Zhang and Y. Kong, *Mater. Res. Bull.*, 2024, **173**, 112697.
7. X. Wang, Y. Jin, N. Li, H. Zhang, X. Liu, X. Yang, H. Pan, T. Wang, K. Wang, D. Qi and J. Jiang, Angew. Chem. Int. Ed., 2024, **63**, e202401014.

8. Y. Luo, C. Liu, J. Liu, X. Liu, Y. Zhou, X. Ou, B. Weng, J. Jiang and B. Han, *Chem. Eng. J.*, 2024, **481**, 148494.
9. S. Feng, H. Cheng, F. Chen, X. Liu, Z. Wang, H. Xu and J. Hua, *ACS Catal.*, 2024, **14**, 7736-7745.
10. D. M. Xue, Y. J. Zhang, J. W. Chen, H. Yang, R. J. Xie, S. C. Qi, Y. Q. Bu, F. Liu, H. H. Zhang and J. Lalevée, *Chem. Eng. J.*, 2024, **502**, 157874.
11. Y. Chen, R. Liu, Y. Guo, G. Wu, T. C. Sum, S. W. Yang and D. Jiang, *Nat. Synth.*, 2024, **3**, 998-1010.
12. Z. Ding, J. Yang, Z. Wu, M. Adeli, X. Luo, X. Wang, X. Xie, X. Xu, C. Cheng and C. Zhao, *Chem. Mater.*, 2025, **37**, 1972-1982.
13. C. Qin, X. Wu, L. Tang, X. Chen, M. Li, Y. Mou, B. Su, S. Wang, C. Feng, J. Liu, X. Yuan, Y. Zhao and H. Wang, *Nat. Commun.*, 2023, **14**, 5238.
14. X. Bai, L. Guo, T. Jia and Z. Hu, *J. Mater. Chem. A*, 2024, **12**, 13116-13126.
15. X. Wang, H. Li, S. Zhou, J. Ning, H. Wei, X. Li, S. Wang, L. Hao and D. Cao, *Adv. Funct. Mater.*, 2025, 2424035.
16. Y. Zhang, Y. Wu, H. Ma, Y. Gao, X. Fan, Y. Zhao, F. Kang, Z. Li, Y. Liu and Q. Zhang, *Small*, 2025, 2500674.
17. S. Chai, X. Chen, X. Zhang, Y. Fang, R. S. Sprick and X. Chen, *Environ. Sci.: Nano*, 2022, **9**, 2464-2469.
18. M. Deng, L. Wang, Z. Wen, J. Chakraborty, J. Sun, G. Wang and P. Van Der Voort, *Green Chem.*, 2024, **26**, 3239-3248.
19. X. Ding, T. Wang, B. Yu, Q. Zhi, H. Wang, H. Liu, P. A. Stuzhin and J. Jiang,

Adv. Funct. Mater., 2025, 2422291.

20. F. Liu, P. Zhou, Y. Hou, H. Tan, Y. Liang, J. Liang, Q. Zhang, S. Guo, M. Tong and J. Ni, *Nat. Commun.*, 2023, **14**, 4344.
21. Z. Li, B. Cai, Y. Zou, D. Zhang, Y. Liang, Y. Zhou, Y. Ma, X. Wang, B. Shi, W. K. Chen, Y. Liu and X. Zhao, *Adv. Energy Mater.*, 2025, DOI: 10.1002/aenm.202500341.
22. L. Zhai, Z. Xie, C.-X. Cui, X. Yang, Q. Xu, X. Ke, M. Liu, L.-B. Qu, X. Chen and L. Mi, *Chem. Mater.*, 2022, **34**, 5232-5240.
23. J. N. Chang, Q. Li, J. W. Shi, M. Zhang, L. Zhang, S. Li, Y. Chen, S. L. Li and Y. Q. Lan, *Angew. Chem. Int. Ed.*, 2023, **62**, e202218868.
24. H. Cheng, H. Lv, J. Cheng, L. Wang, X. Wu and H. Xu, *Adv. Mater.*, 2022, **34**, 2107480.
25. D. Chen, W. Chen, Y. Wu, L. Wang, X. Wu, H. Xu and L. Chen, *Angew. Chem. Int. Ed.*, 2023, **62**, e202217479.
26. X. Di, X. Lv, H. Wang, F. Chen, S. Wang, G. Zheng, B. Wang and Q. Han, *Chem. Eng. J.*, 2023, **455**, 140124.
27. J. Chen, S. Yan, F. Wang, F. Lin, J. Lin, R. A. Borse and Y. Wang, *Angew. Chem. Int. Ed.*, 2025, **64**, e202500924.
28. D. Cao, J. Du, J. Li, Q. Sun, J. Guan and J. Liu, *ACS Catal.* , 2025, **15**, 3584-3594.
29. C. Shu, X. Yang, L. Liu, X. Hu, R. Sun, X. Yang, A. I. Cooper, B. Tan and X. Wang, *Angew. Chem. Int. Ed.*, 2024, **63**, e202403926.

30. R. Sun, X. Hu, X. Yang, Y. Guo, C. Shu, X. Yang, H. Gao, X. Wang and B. Tan, *Chem. Eng. J.*, 2024, **490**, 151332.